Modeling proton transfer and polarons in a molecular crystal diamino-dinitroethylene

Anna V. Kimmel,[1,2,*] David Muñoz Ramo,[2,†] Peter V. Sushko,[2] Alexander L. Shluger,[2] and Maija M. Kuklja[3]
[1]*Department of Physics, University of Nevada Las Vegas, Las Vegas, Nevada 89154, USA*
[2]*Department of Physics and Astronomy and the London Centre for Nanotechnology, University College London, Gower Street, London WC1E 6BT, United Kingdom*
[3]*Department of Materials Science and Engineering, University of Maryland, College Park, Maryland 20742, USA*
(Received 24 March 2009; revised manuscript received 20 June 2009; published 7 October 2009)

We applied embedded cluster and periodic methods to modeling the intramolecular and intermolecular hydrogen transfer and electron and hole trapping in a crystalline 1,1-diamino-2,2-dinitroethylene (DADNE) by means of density-functional theory and B3LYP functional. We predict self-trapping of both electrons and holes to occur and be accompanied by a strong lattice distortion in perfect DADNE crystals. The results also demonstrate that a combination of periodic and embedded-cluster techniques serve as a powerful simulation tool for revealing intricate details of the proton transfer in molecular crystals.

DOI: 10.1103/PhysRevB.80.134108 PACS number(s): 61.50.Ah, 61.66.Hq, 61.72.Bb

I. INTRODUCTION

Chemical reactions, photoexcitations, as well as carrier localization and transport processes in molecular crystals are important for their diverse technological applications in electronics, as organic dyes, energetic materials, in electrophotography and in many other areas. Atomistic modeling of these phenomena is challenging due to complexity of molecular and crystalline structures, and large number of configurations available to molecules and reaction products. Quantum-mechanical calculations of molecular materials have been carried out either for individual molecules and small molecular aggregates (see, for example, Refs. 1–5) or using periodic models (e.g., Refs. 6–8 and references therein). Electrons are often well localized on individual molecules and therefore the constituting molecules largely preserve their identity in molecular solids.[9,10] This lends some support to molecular calculations, which are often considered to be a reliable first step in modeling. Although this approach indeed provides useful preliminary information of the materials' properties, it clearly neglects the intermolecular interactions and crystal-field effects, which are particularly important when molecules are polar or possess nonzero dipole moment creating long-range electrostatic field in the system. These effects can be taken into account in the periodic model. However, using this model encounters difficulties when considering reactions involving charge transfer, electron and/or hole localization and excited states.[11–13]

The hybrid "embedded cluster" and quantum-mechanical/molecular-mechanical (QM/MM) methods have long been used to study defects and reactions in solids involving charged and excited states (see, for example, Refs. 14 and 15). They combine quantum-chemical methods for describing part of the system with classical treatment of the rest of the system and are extensively used to describe crystalline as well as disordered solids[16] and bio-molecules.[15,17,18] Surprisingly, applications of these techniques to molecular crystals are scarce. This is in spite of the fact that the intermolecular interactions in many molecular materials are much weaker than intramolecular interactions and, therefore, these systems can be easily divided into regions, treated at different levels of theory and amenable to QM/MM. Recently, a QM/MM method has been applied to study the structure of a range of organic molecular crystals.[19] At present, we are unaware of any applications of this method to studying defects in molecular crystals, where it may have significant advantages with respect to molecular and periodic models.

In this paper, we use both a periodic and an embedded cluster method (ECM) to model defects and defect-induced processes in molecular solids. We employ a self-consistent ECM technique implemented in the GUESS code.[20] This method has been previously applied extensively to studying defects in the bulk and at surfaces of ionic insulators.[16] We show that the same approach can be used to study molecular crystals. We then apply the method to study the hydrogen transfer as well as electron and hole polarons in a molecular energetic crystalline material 1,1-diamino-2,2-dinitroethylene (DADNE). DADNE crystal is composed of nonplanar molecules [Fig. 1(a)] arranged into zigzag parallel layers [Fig. 1(b)].[21] DADNE molecules possess a nonzero dipole moment and the interaction between dipoles makes a significant contribution into the cohesive energy.

The hydrogen transfer and electron and hole trapping are examples of relevant problems in energetic and, more generally, molecular materials, which are difficult to tackle using periodic or molecular models alone. Our ECM modeling of the hydrogen transfer in DADNE revealed that it is essentially a collective phenomenon and cannot be properly understood when simulated by molecular models that neglect the crystalline environment and the interaction between molecules. Our periodic and ECM calculations also demonstrate that both an extra electron and hole can be self-trapped in perfect DADNE crystal due to their interaction with the lattice. This is important for the understanding of the electronic properties of organic insulators and molecular crystals and, as we demonstrate below, is difficult to model using periodic boundary conditions.

The rest of the paper is organized as follows. In the next section, we describe the embedded-cluster method and the computational details. In Sec. III, we test the accuracy of this method and our computational scheme, and in Sec. IV, we discuss the results of calculations for hydrogen transfer and

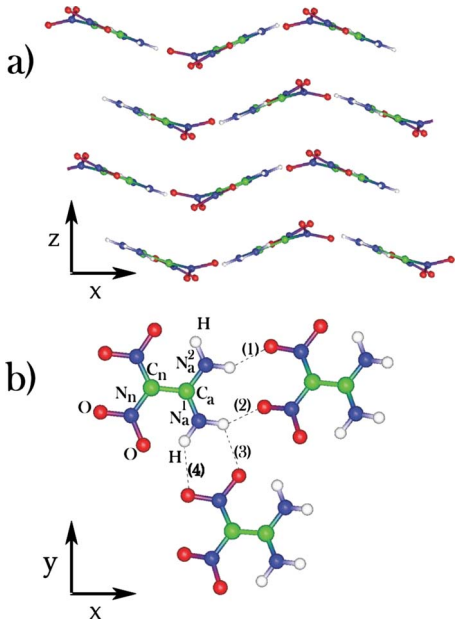

FIG. 1. (Color online) The crystalline structure of DADNE. (a) Molecules are arranged into parallel polar layers; (b) the in-layer molecular arrangement demonstrates the hydrogen bond network. Broken lines (1), (2), (3), and (4) show nonequivalent connections of nitro (O-N_n-O) and amino (H-N_a-H) groups along which intermolecular hydrogen transfer may occur. Atoms related to amino and nitro groups are denoted with lower index "a" or "n," respectively.

electron and hole trapping in DADNE. Our conclusions are summarized in Sec. V.

II. METHODS OF CALCULATIONS

Most of our calculations are performed using the ECM method and the GUESS code.[20] We also use periodic calculations and the CRYSTAL06 code[22] to test or complement some of our predictions. Within the ECM method, a crystal is represented with a finite system, which is divided into a relatively small region of interest, described quantum mechanically, and the rest of the system treated classically using the shell model or rigid classical ions.[15,20] The challenging part of this approach is the description of the bonded interactions at the border between the QM and classical subsystems.[14,20] In molecular crystals, such as DADNE, the molecules are often linked together by the electrostatic and van der Waals (vdW) interactions and by hydrogen bonds. The absence of bonded intermolecular interactions makes the description of the border between quantum and classical regions simpler than in the case of covalent or semicovalent systems where special semilocal embedding pseudopotentials are needed.[23] Below we demonstrate that an approach developed for ionic and atomic systems[20] can serve as a first approximation for describing the electronic structure and defects also in molecular crystals.

A. General setup of ECM

The ECM takes into account the electrostatic interaction of the electrons and nuclei inside the QM cluster with the

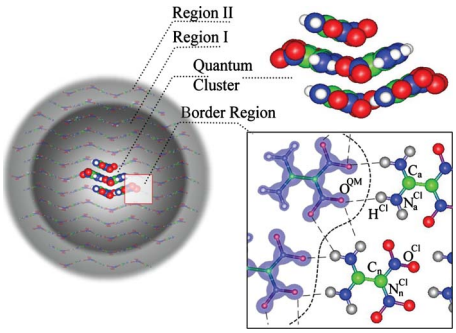

FIG. 2. (Color online) A schematic representation of the Embedded Cluster Model. The quantum cluster is shown in the center of the fully relaxed region I, which is surrounded by the constrained region II. The blown-up region shows the interface between the quantum and classical regions.

rest of the host lattice, the perturbation of the lattice by the defect (by displaced hydrogen, extra electron, and absence of electron in our case), and the reciprocal effect of the lattice polarization on the defect itself. In application to molecular crystals, the system can be subdivided into several regions corresponding to different scales, as shown on Fig. 2. Region I includes several hundred molecules with a QM cluster at the center. The QM cluster includes an integer number of molecules and is chosen in such a way that to have zero dipole moment in order to avoid artificial electrostatic effects. The positions of all atoms in region I are optimized using the standard Broyden-Fletcher-Goldfarb-Shanno (BFGS) algorithm.[24]

Region I is surrounded by a finite region II, which comprises several thousand molecules, where atoms are kept fixed in their ideal positions in the crystalline lattice. The role of this region is to mimic the infinite crystalline environment and provide correct representation of the electrostatic potential and short-range intermolecular interactions inside region I. The matrix elements of the electrostatic potential produced by regions I and II are included into of the Kohn-Sham equations, which are solved for the electrons in the QM cluster. In addition, the non-Coulomb short-range interactions between the molecules in regions I and II are included to provide correct boundary conditions for calculations of geometric structure of QM cluster.

The total energy of the whole system is given by:

$$\mathbf{E} = \mathbf{E_{QC}} + \mathbf{W_{QC+CL}} + \mathbf{E_{CL}},$$

where E_{QC} is the energy of the QM cluster in the electrostatic potential of the rest of the crystal; W_{QC+CL} describes the energy of non-Coulomb interactions between the quantum atoms inside the QM cluster and classical atoms in region I; E_{CL} is the total energy of the classical environment (perturbed by a defect inside the QM cluster). The quantum-mechanical contributions to the total energy and forces are calculated using the GAUSSIAN03 package.[25] In the calculations described below, we used the hybrid B3LYP density functional.[26,27]

A method of calculation of W_{QC+CL} is central to all ECM techniques and strongly depends on the system. The aim here

is to make sure that electrons at the border of a QM cluster are described correctly and do not experience any artificial perturbations caused by the fact that part of their neighbors are classical atoms. The latter may cause spurious electron polarization toward positively charged classical ions and other undesirable effects. To avoid that, in ionic crystals, positive ions surrounding a QM cluster are usually represented by their full ion pseudopotentials.[20] In this work, in the first approximation, the atoms constituting the molecules outside the QM cluster are treated classically and no embedding pseudopotentials are introduced. However, the classical interaction of the atoms inside the QM cluster with those outside the QM cluster is included via the same short-range interatomic potentials as in the classical part of region I (*vide infra*). Tests presented in the next section demonstrate that this is a reasonable approximation for the type of problems considered in this work.

To choose an appropriate basis set, we have performed a series of molecular and ECM calculations. For molecular calculations, we have tested split valence basis sets 6-21G, 6-31G, 6-31+G*, 6-31+G**, and the extensive correlation consistent basis set cc-pVTZ. We have found that the 6-31+G** basis set provides the best compromise between the accuracy and efficiency in molecular calculations.

In solid state *ab initio* calculations, the basis set is effectively richer due to interference between the basis functions of different centers. Testing 6-21G, 6-31G, 6-31+G*, 6-31+G** basis sets in ECM calculations demonstrated that increasing the basis set beyond 6–31G induces a pseudolinear dependence "catastrophe,"[28] and the 6-31G and the 6-21G basis sets yield a negligible difference in the electronic structure of the system. This is consistent with a general trend[29] and with the earlier careful tests performed for several energetic crystals.[30–32] Therefore, in ECM calculations, we used the 6-21G basis set.

The DFT method used in this work does not fully include the vdW interaction between molecules. In order to estimate the significance of the vdW contribution in determining the properties of DADNE, we have compared the interaction energy profiles obtained for two DADNE molecules using B3LYP (Refs. 26 and 27) and a recently developed density functional (vdWDF).[33] We have found that B3LYP and vdWDF give very similar equilibrium geometries of DADNE molecules and distances between molecules. Since in periodic calculations we are mostly concerned with differences between total energies of the initial and final states of the system, it seems reasonable to assume that neglecting the vdW interactions will hardly affect our conclusions. In ECM calculations, region II is fixed in the perfect lattice geometry and cohesive energy is not considered. The vdW contribution is not accounted for only within the QM cluster. Therefore relative energies should be even less affected. The recent study of a series of molecular materials lends a strong support to this approximation.[34] Nevertheless, taking into account the vdW interaction may prove to be more important for other molecular solids and can be achieved, for example, by including a damping function[35,36] or empirical terms into the Hamiltonian.[33]

B. Force field

Different force fields are used for describing the intermolecular and intramolecular interactions in region I. The intramolecular interactions are described by pairwise Morse potentials, three-body bending potentials, and four-body torsion potentials. In the current scheme, the Coulomb interactions inside the molecules are effectively accounted for by pairwise Morse potentials. The parameters of the intramolecular potentials[37] were fitted to reproduce the structure and vibrational frequencies of isolated molecule and the crystalline structure obtained using the B3LYP density functional.

The intermolecular interactions include the Coulomb interaction, the hydrogen-oxygen interaction within the molecular layers and the vdW interaction. To account for the Coulomb interaction, each atom in the classical regions I and II is assigned a partial charge obtained from *ab initio* calculations using a natural population analysis (NPA),[38] as implemented in the GAUSSIAN03 code. Then, the classical charges were iteratively optimized to provide a consistent set of ionic charges in the quantum cluster and the classical environment. The obtained classical ionic charges on nitrogen atoms are fairly close to those in the QM cluster; the average values of quantum charges on hydrogen and oxygen atoms differ from those in the classical environment by only 0.05–0.08 e; the

TABLE I. Geometry parameters of a single DADNE molecule and a molecule in the crystalline environment. Bond lengths are given on angstroms, Å, bending and torsion angles are in °.

Parameter	Gas phase	ECM eight molecules	Periodic	Experiment (Ref. 21)
C=C	1.43	1.47	1.49	1.46
C-N_a	1.34	1.32	1.34	1.32/1.325
C-N_n	1.43	1.41	1.41	1.4/1.426
N_a-H	1.002/1.008	1.01	1.04	0.84
N_n-O	1.23/1.26	1.3	1.32	1.25
intramolecular H-O	1.75	1.75/1.8	1.76/1.81	1.97/2.03
$\angle N_a$-C-N_a	117.32	117.78	119.8	118.4
$\angle N_n$-C-N_n	116.63	118.54	117.5	116.21
$\angle N_a$-C_a-C_n-N_n^1	−12.6	−4.7/−7.0	−3.5	−4.0
$\angle N_a$-C_a-C_n-N_n^2	167.3	174.2/177.8	176.8	177.0

TABLE II. Effective atomic charges used for nonbonding interactions in DADNE simulations.

	Effective atomic charges, $\|e\|$
C_a	+0.44
C_n	+0.06
N_a	−0.83
N_n	+0.48
H_1/H_2	+0.48/+0.43
O_1/O_2	−0.34/−0.47

quantum charges on carbon ions attached to nitro groups are slightly larger (by 0.12 e) than those in the QM cluster due to effectively richer basis set. This charge set provides the stable geometry and the correct electronic structure of the modeled system, as will be illustrated below.

The parameters for nonbonded intermolecular Lennard-Jones potentials were initially obtained for rigid DADNE molecules[39] and readjusted in this work to achieve consistency with the used model of fully flexible molecules and the set of effective charges. The H-O interactions are described by Lennard-Jones potentials fitted to the results of *ab initio* calculations of the interaction energy between two DADNE molecules within one molecular layer. This force field reproduces correctly the geometry of the crystalline DADNE (see Table I). For example, the intramolecular torsion angles [see Figs. 1(a)] $\angle N_n\text{-}C_a\text{-}C_n\text{-}N_a^1$ and $\angle N_n\text{-}C_n\text{-}C_a\text{-}N_a^2$ for DADNE molecules in the QM cluster are equal to −4.7° and −178°, in good agreement with their experimental values of −4.7° and −177°, respectively.

The structure of molecular crystals is to a large extent determined by the hydrogen bonds between the molecules. The positions of light hydrogen atoms are determined indirectly from x-ray experiments. At the same time, the intermolecular distances between amino nitrogen and nitro oxygen, $N_a\text{-}O_n$, are measured directly and can serve as a good parameter for characterizing the hydrogen network. The experimental values of $N_a\text{-}O_n$ in crystalline DADNE are 3.0 and 2.61 Å (Ref. 21) whereas our force field provides values of 3.03 and 2.69 Å. The parameters of the force field used in this paper are summarized in Tables II–VI. Before considering the applications of this technique, we describe the results of tests performed to justify the validity of approximations made and compare the properties of isolated molecules with those in the crystalline environment described by ECM.

TABLE III. Intramolecular Morse potentials $U=F\{1-\exp[-\alpha(r-r_0)]\}^2$.

Atoms	F (eV)	r_0 (Å)	α (Å^{-1})
$C_a\text{-}N_a$	3.17	2.67	1.34
$N_a\text{-}H$	4.03	2.10	1.01
$C_a\text{-}C_n$	6.33	1.57	1.43
$C_n\text{-}N_n$	2.91	1.80	1.43
$N_n\text{-}O$	6.20	1.94	1.24

TABLE IV. Intramolecular three-body bending potentials $U=1/2k_B(\theta\text{-}\theta_0)^2$.

Atoms	k_B (eV/rad^2)	θ_0 (deg)
$H\text{-}N_a\text{-}H$	2.63	121.58
$H\text{-}N_a\text{-}C_a$	3.15	117.76
$N_a\text{-}C_a\text{-}N_a$	10.26	117.57
$N_a\text{-}C_a\text{-}C_n$	6.28	121.21
$N_n\text{-}C_n\text{-}C_a$	5.71	121.58
$N_n\text{-}C_n\text{-}N_n$	12.35	116.84
$C_n\text{-}N_n\text{-}O$	4.78	118.81
$O\text{-}N_n\text{-}O$	9.93	122.35

C. Properties of the perfect lattice

The quality of embedding can be assessed by comparing the results of ECM calculations with those obtained using periodic boundary conditions and a similar computational method. In this case, it is convenient to use the CRYSTAL06 code,[22] which employs the same density functional and basis set as used by the ECM. In order to check how the ECM results depend on the QM cluster size, we have performed a series of calculations using QM clusters containing m molecules (m=4, 6, 8, and 14), further denoted as QC_m. The QC_4 cluster [See Fig. 3(a)] replicates the crystalline unit cell and has zero dipole moment due to symmetry. QC_6 and the QC_8 [Figs. 3(b) and 3(c)] have been chosen to model chemical reactions and charge transfer between two molecules as they provide the quantum environment for the intermolecular space between two molecules. Finally, in QC_{14}, the central DADNE molecule is fully surrounded by molecules treated quantum mechanically, which should allow us to model structural defects, such as molecular vacancy, stereo isomers etc., and chemical reactions in future studies.

We found that the size and topology of QM clusters have negligibly small effects on the equilibrium geometry of molecules inside the QM cluster. We have observed only a small elongation of C=C bonds by about 0.005 Å with the increase in the QM cluster size while the rest of the intramolecular parameters remained the same as in the perfect crystal calculated using the CRYSTAL code. At the same time, the

TABLE V. Intramolecular four-body torsion potentials $U=k_T[1-\cos(\varphi\text{-}\varphi_0)]$.

Atoms	k_T (eV)	φ_0 (deg)
$H\text{-}N_a\text{-}C_a\text{-}N_a$	0.31	−17.25
$H\text{-}N_a\text{-}C_a\text{-}C_n$	0.46	+1.80
$N_a\text{-}C_a\text{-}C_n\text{-}N_n$	0.07	−13.50
$O\text{-}N_n\text{-}C_n\text{-}N_n$	0.90	+23.60
$O\text{-}N_n\text{-}C_n\text{-}C_a$	0.25	+21.40
$N_a\text{-}H\text{-}H\text{-}C_a$	0.00	+12.80
$N_n\text{-}O\text{-}O\text{-}C_n$	6.60	+1.43

TABLE VI. Intermolecular Lennard-Jones potentials $U = A/R^{12} - B/R^6$.

Atoms	A (eV Å^{12})	B (eV Å^6)	R_{cutoff} (Å)
C-C	67800.0	44.26	50.00
H-O	29.8	0.90	2.50
O-O	5500.0	15.30	50.00
N-N	60000.0	27.00	50.00
H-H	930.2	2.17	50.00

variations in the interlayer C-C and N-N distances with respect to the cluster size do not exceed 0.03 Å. However, due to a small difference between charges on the atoms inside the QM cluster and in the classical regions I and II, the intermolecular H-O distances between classical and quantum molecules on average are slightly longer (0.15 Å) than these in the perfect crystal. The dispersion of these distances is 0.1 Å.

The cluster size does not affect significantly the nature of electronic states forming the top of the valence band and the bottom of the conduction band. The highest occupied molecular orbital-lowest unoccupied molecular orbital (HOMO-LUMO) band gap as a function of the QM cluster size varies from 3.3 to 3.54 eV. This is caused by the difference in topologies of the QM clusters (see Fig. 3).

The geometric parameters of molecules, including equilibrium bond lengths, angles, and torsion angles, obtained using different techniques are summarized in Table I together with the experimental data. We note that our molecular calculations are consistent with the previously reported results.[3,4] As expected, our *ab initio* periodic and ECM calculations of the geometry agree well with the experiment[21] and earlier periodic calculations,[40] however, slightly differ from the molecular geometry in the gas phase.[2] The most significant difference is the length of the C=C bond, where the value obtained via ECM is consistent with experiment[21,40] and periodic calculations.[40] We note that, due to the inclusion of the crystalline field in the method, the torsion angles N_a-C_a-C_n-N_n in ECM calculations are in a better agreement with the experimental parameters then those for a single molecule [See Table I and Fig. 2(a)].

To test further the effect of the boundary between the quantum cluster and the classical region on the nature of electronic states, we calculated the electronic structure of the perfect QC_8 cluster with an excess electron. In the perfect frozen lattice, the extra electron should delocalize equally between the molecules of the QM cluster. Hence, should the electron localize preferentially on one group of molecules or tend to escape outside the cluster being attracted by positively charged classical ions, this would indicate that our embedding method does not work properly. On the other hand, the artificial delocalization could manifest itself in the HOMO having strong contributions of the most diffuse primitive orbitals extending outside the cluster. Notably, our results demonstrate that the extra electron is fully delocalized over the quantum cluster almost equally occupying the molecular orbitals of nitro groups. Also, we have not found excessive occupation of the diffuse functions of quantum oxygen ions that might indicate the artificial polarization at the border. This is because the negatively charged classical oxygen and nitrogen atoms surrounding the QM cluster repel an extra electron and effectively screen the positively charged hydrogen atoms, as appropriate, and prevent artificial spreading of the electron density outside the QM cluster. These tests assured that the ECM in the developed implementation accurately reproduces the basic properties of ideal DADNE lattice.

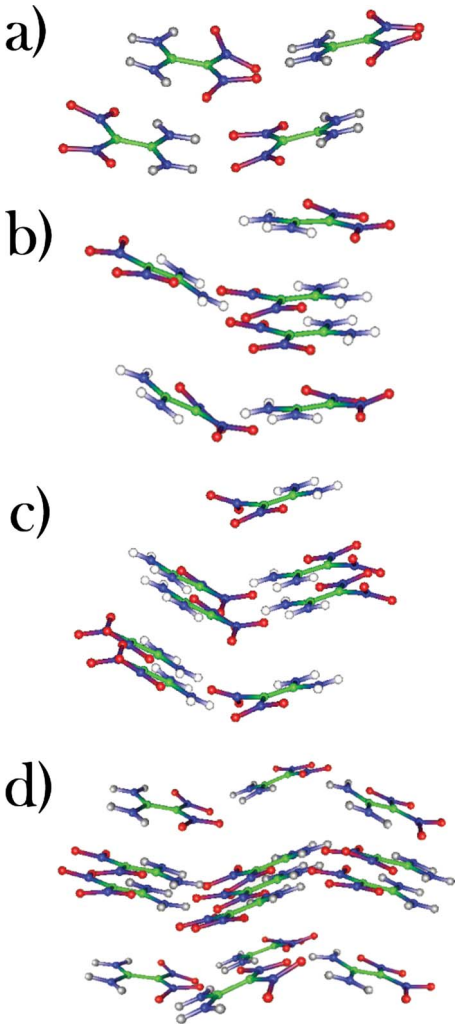

FIG. 3. (Color online) Quantum clusters used in ECM calculations differ in their shapes and topologies due to symmetrical and zero net dipole moment considerations: (a) The four-molecule QM_4 cluster represents the DADNE unit cell; (b) The six molecule QM_6, (c) the eight molecule QM_8 clusters include molecules from three adjacent molecular layers, which is necessary to model a hydrogen transfer process; and (d) The 14 molecule QM_{14} cluster is constructed in such a way that the central DADNE molecule is fully surrounded by its quantum-mechanical molecular neighbors.

D. Molecule versus crystal

As discussed in the Introduction, a number of previous calculations for DADNE have been carried out using isolated

molecules.[2–4] Since a significant part of the effect of the crystalline environment stems from the electrostatic interaction with the molecules constituting the lattice, it is illuminating to evaluate the contribution of the surrounding molecules into the on-site electrostatic potential (EP) on atoms constituting each molecule. For this purpose we calculated the EP on atoms in an isolated DADNE molecule and in a molecule embedded in the crystalline environment described by both EMC and periodic models. All three types of classical calculations were performed using the GULP code[41] and the NPA atomic charges obtained using GAUSSIAN03 calculations for a single molecule with the B3LYP functional and an extended basis set.

These calculations reveal strong variations in the EP within an individual molecule, with the 20 V difference in the value of the EP between nitrogen atoms belonging to amino and nitro groups and with the lowest EP on the oxygen ions [See Fig. 4(a)]. The importance of EP for properties of organic molecules was pointed out earlier for a series of materials.[42] The relative values of the EP on the same atoms in a molecule inside a perfect crystal demonstrate the effect of the crystalline environment. These values for the individual molecule and for the periodic lattice are presented in Fig. 4(b). They demonstrate an about −3 V shift of the EP value on the hydrogen atoms due to the crystalline environment, whereas the EP on oxygen atoms is shifted only by 0.2–2 V.

Ideally, the EP values should be equal in the periodic and ECM models. The difference between the EP values in the cluster and periodic models is quite small for carbon ions and nitro groups. For hydrogen ions, this difference reaches 0.3 V, which is small with respect to the absolute values of the potential on the site [see Fig. 4(c)]. This difference stems from the finite size of the quantum cluster used in the EMC calculations and the fact that it has a nonzero quadruple moment.

Further, we have performed the analysis of the electronic structures of a single DADNE molecule, a periodic DADNE crystal and a QM cluster embedded into the classical crystalline environment. We found that the splitting between the HOMO and the LUMO in a single molecule is 4.77 eV (See Fig. 5 and Ref. 2). The energy gap between the occupied and unoccupied electronic states decreases in the solid due to intermolecular interactions. Indeed, the band gap obtained in the periodic CRYSTAL calculations is equal to 3.46 eV [Fig. 5(b)]. The ECM calculations for the quantum cluster containing eight molecules give 3.44 eV [see Fig. 5(c)]. These results are consistent with the band gap of 3.4 eV obtained in earlier calculations by the Hartree-Fock method and corrected for electronic polarization by many-body perturbation theory.[43]

Further analysis of the nature of occupied and unoccupied states in a single DADNE molecule demonstrates similarities with the states forming the top of the valence and the bottom of the conduction band in the solid DADNE. Indeed, the HOMO in both the single molecule and the perfect crystal is formed predominantly by the atomic orbitals of carbon atoms and oxygen atoms of the nitro groups with a small contribution from nitrogen atoms of the amino groups. The lower lying HOMO-1 state is formed by the atomic orbitals

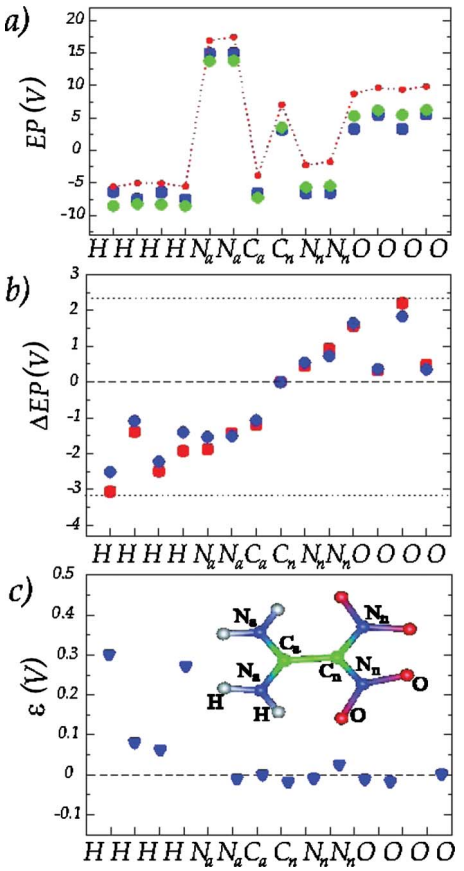

FIG. 4. (Color online) The electrostatic potential difference on atoms of a DADNE molecule. (a) EP calculated for a single DADNE molecule (red circles), a molecule in the center of nanocluster (blue squares) and a molecule in perfect crystal (green diamonds). One can see that influence of the crystalline field is reflected in the shift of the EP for nanocluster and periodic model with respect to a single molecule. (b) The relative difference in electrostatic potential between molecular and cluster models (red squares), and between molecular and periodic models (blue circles). One can see that the functional groups are more affected by the crystalline field: the magnitude of EP deviation reaches 3 V for nitro and amino groups. (c) The relative difference, ε, between electrostatic potentials in periodic and cluster models. This plot demonstrates the error in reproducing the electrostatic potential in an infinite crystal modeled by a finite cluster. The largest deviation in EP on hydrogen ions is 0.3 V, which is small in comparison with absolute values of EP.

of the oxygen atoms of the nitro groups. The HOMO-2 state is formed by the states of nitrogen of amino and nitro groups, and oxygen atoms.

One can note also some differences between the electronic states of a single molecule and the DOS of the crystalline DADNE obtained in periodic and ECM calculations [see Figs. 5(a)–5(c)]. There is a good correspondence between the highest occupied levels of a DADNE molecule and the top of the valence band of crystalline DADNE. However, in the crystal, a level at the energies below −10 eV formed by hydrogen atoms split from the deeper states [Figs. 5(b) and 5(c)]. This is due to the intermolecular interactions of hydrogens with nitrogen and oxygen atoms, which is charac-

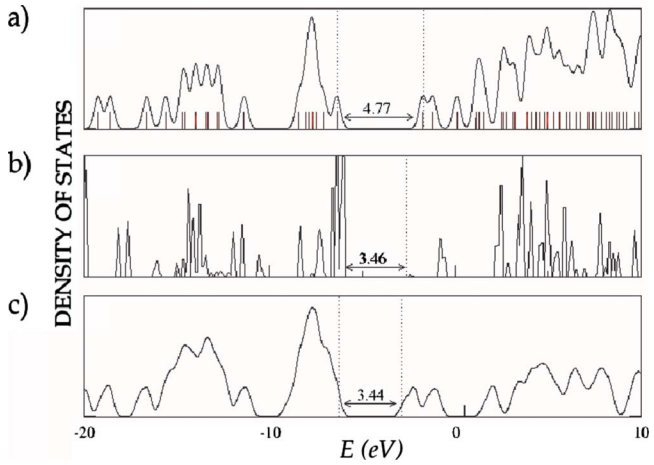

FIG. 5. (Color online) One-electron energy spectrum of a single DADNE molecule (a) is compared to the density of states of a perfect DADNE crystal obtained from (b) *ab initio* periodic calculations, and (c) ECM calculations. The nature of the states forming the bands is discussed in the text.

teristic for the crystalline environment. One can see that this feature of the DOS is also reproduced in the ECM calculations.

The lowest unoccupied levels of a single molecule, LUMO and LUMO+1, are formed by the states of nitro groups. In the perfect crystal, these levels correspond to the subband in the conduction band at −1.5 eV. This feature is well reproduced in both the periodic and ECM calculations. The next unoccupied level of a single molecule, LUMO+2, is formed by a mixture of hydrogen and nitrogen atomic orbitals. In the crystal, this level corresponds to a subband in the conduction band. However, its position in the ECM model is shifted in comparison to that in the periodic model. This is an artifact of the boundary conditions, where the interactions of quantum hydrogen atoms with the classical atoms at the QM cluster border contribute to the energy and effectively lower the position of these electronic levels.

Thus, the most substantial effect of the intermolecular interactions evident so far is the smaller crystalline band gap (3.4 eV) as compared to the gas phase HOMO-LUMO gap (4.8 eV) and certain perturbations of deep valence-band levels and relative shift of unoccupied levels. This implies that, in spite of the fact that the electron density of the system is well localized on individual molecules, the interaction between them in the crystalline matrix is non-negligible, especially for considering higher electronic excitations, whose energies may be estimated incorrectly in a molecular approach.

III. HYDROGEN TRANSFER IN DADNE

Several experimental reports provide indirect evidence for the hydrogen transfer in DADNE. The presence of water and NO species among the DADNE decomposition products[44,45] also suggests that the hydrogen transfer could act as a potential precursor for its overall thermal decomposition. We define the hydrogen-transfer process hereafter as a short-distance migration of a hydrogen atom (or ion) from an amino to a nitro group either within a single molecule or between two nearest-neighbor molecules (see Fig. 6), which is accompanied by hydrogen bond switching (N-H---O → N---H-O). Note, in this study, we did not consider "global" proton transfer, which involves H-bond wires and may be coupled to global structural rearrangements (see, for instance, Ref. 46).

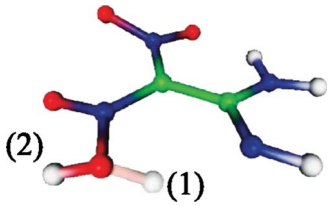

FIG. 6. (Color online) Two HONO-DADNE molecular isomer configurations are shown: the location (1) of hydrogen atom is unstable due to insufficient electronegativity of oxygen relative to the host nitrogen atom; the proton finds a metastable location (2) by attaching to the nitro group.

One of the possible configurations of a hydrogen atom attached to the neighboring nitro group (H-O-N-O formation) within the same molecule is shown in Fig. 6. In our ECM calculations, it proved to be unstable. The potential-energy profile along the direction from amino to nitro group demonstrates a monotonous energy increase with no local minimum. Therefore hydrogen returns back into its initial position in the molecule when relaxed at any position on this path.

According to the NPA analysis, hydrogen is in a positive charge state in all the configurations along the transfer path. The redistribution of the electron density on atoms due to the broken N-H bond confirms that the electron density remains mostly localized at the host nitrogen atom (its atomic charge changes from −0.7 to −0.9 e) and only a small amount of it is delocalized over oxygen atoms. Hence, the strong electrostatic interaction between the H^+ and the host N^- ions precludes the hydrogen transfer. This conclusion is consistent with the previous calculations of individual DADNE molecules, where no hydrogen transfer with the formation of a stable HONO isomer has been observed.[2]

Searching for other intramolecular hydrogen transfer paths, we have found a local energy minimum corresponding to a metastable HONO arrangement [see configuration (2) in Fig. 6] in which the hydrogen atom is located between the two oxygen atoms of a nitro group. The energy of this configuration is, however, by 1.98 eV higher than the perfect lattice energy. There is no obvious short-distance pathway for hydrogen to travel from the host amino group to this local minimum configuration, which would be consistent with switching of hydrogen bonds (Fig. 6). Using a nudged elastic-band method[47] we have found that the system needs to overcome a barrier of 4 eV to reach this minimum. The proton-migration path passes by the nitro carbon due to its relatively small positive charge. At the transition state, the proton is at 1.3 Å over the carbon ion. Then, after passing positively charged nitrogens of neighboring nitro groups, proton reaches the area, where the adiabatic potential profile

has a descending character due to the high electron density supplied by oxygen ions, and finds a stable position between them.

We note that the calculated barrier is much higher than the experimental estimate of the thermal-activation energy of DADNE decomposition of 58 kcal/mol.[44] Therefore, HONO formation does not seem to be a feasible candidate for the thermal initiation of DADNE decomposition under gentle thermolysis conditions. However, proton can occur in this configuration as a result of the hydrogen diffusion in the crystal or due to another high-energy process, for example, shock or irradiation.

In order to study the intermolecular hydrogen transfer, we have considered several in-layer directions as shown by broken lines in Fig. 1(a), and again constructed a mesh of initial guesses for the hydrogen positions. Regardless of the initial guess, hydrogen relaxed back into the initial geometry and did not form a stable HONO configuration with neighboring molecules. Thus, the results of our calculations demonstrate that intermolecular transfer does not take place in crystalline DADNE either.

Our results demonstrate that the hydrogen transfer and following HONO formation hardly play an important role in the thermally activated initiation chemistry of DADNE contrary to earlier predictions.[44] We note that proton transfer in hydrogen-bonded materials is a common process, which has been modeled using several methods (see, for example, Refs. 6–8). As was noted above, the proton separation from the neutral host molecule leads to the formation of a dipole moment between them. The Coulomb attraction of the proton to the negatively charged molecule is the main reason for the high separation barrier in our case. Large periodic cells would be required to eliminate the cell-size effects and the interaction between the periodically translated dipoles. Thus using ECM offers an advantage with respect to periodic calculations in this case.

IV. MODELING ELECTRON AND HOLE POLARONS

Another example of a problem, which benefits from combining ECM and periodic calculations, is electron and hole trapping in insulators.[16] Will carriers undergo free-band propagation or will they instead become self-trapped or trapped by impurities is a basic issue. Polarons in molecular crystals have been a topic of numerous model studies before and after classical work by Holstein and Emin.[48,49] However, many-electron *ab initio* calculations of polarons in these crystals are still scarce (see, for example, Refs. 7, 8, and 50). An answer to a crucial question as to whether or not the carrier is localized depends strongly on the Hamiltonian used in such calculations. It is well established that calculations using the Hartree-Fock approximation tend to localize electrons and holes and these using DFT and local-density approximation (LDA) or generalized gradient approximation (GGA) approximations tend to predict delocalized solutions.[51,52] Therefore making reliable predictions is difficult.

An advantage of using ECM here is that a single extra charge can be modeled using a relatively small QM cluster whereas the polarization of the rest of the solid is accounted for via polarization of the region I. Comparing with experiment requires calculating optical and magnetic characteristics of localized carriers, which is again easier within molecular methods implemented in ECM. Disadvantages are that in ECM, an extra electron or hole is confined to QM cluster and also that perturbations induced by the boundary effects can trigger localization. Therefore this method requires calibration with respect to periodic calculations to reliably establish the character of carrier localization. It is best applied to calculating the spectroscopic properties and diffusion barriers of localized polarons.[16]

Reliable predictions of the character of electron or hole localization in solids require going beyond LDA or GGA approximations of the standard DFT.[51,52] To establish the character of carrier localization one can use a periodic method and DFT with density functional including nonlocal exchange. In particular, using hybrid density functionals proved to be a practical way of including nonlocal exchange interaction necessary for treating localization/delocalization problems.[16,51] Yet, the result can depend on the amount of the Hartree-Fock exchange included in the functional.[16] Below we describe both periodic and ECM calculations of an extra electron and hole in DADNE performed using the B3LYP functional. We note that the only other periodic calculations for polarons in a molecular crystal we are aware of have recently been carried out for polyethylene.[8]

A. Periodic polaron calculations

The periodic CRYSTAL06 calculations employed $2\times2\times1$ and $2\times2\times2$ supercells containing 16 and 32 DADNE molecules, correspondingly. Using these supercells ensures good balance between computational effort and spacing of the periodic images. In addition, Durand-Barthelat effective core potentials with their associated valence basis sets (equivalent to the basis set used in the embedded-cluster calculations) were used for the $1s$ shells of C and O to speed up the convergence process.[53] Eight k points in a Monkhorst-Pack scheme were selected for the k-point mesh.

The electronic structure of DADNE crystal inherits the main features of the molecular electronic structure (see Fig. 5). Indeed, the top of the valence band of the crystal is formed by carbon states and oxygen orbitals of nitro groups; when deeper valence-band levels are formed by the amino groups and carbon atomic orbitals. The bottom of the conduction band is mainly formed by the orbitals of the nitro groups. These states form a narrow band, which is split from the next subband of the conduction band and causes the electron localization described below. In the perfect lattice calculations, an extra electron populates this LUMO state and is delocalized over the nitro groups of the molecules constituting the periodic cell. The excess charge was compensated by a charged background. However, if the lattice relaxation is allowed, the excess electron induces a pronounced lattice distortion accompanied by the electron localization. The extra electron charge is unequally distributed between the two neighboring molecules in adjacent layers. One of them has a larger amount of spin density than the other and it is local-

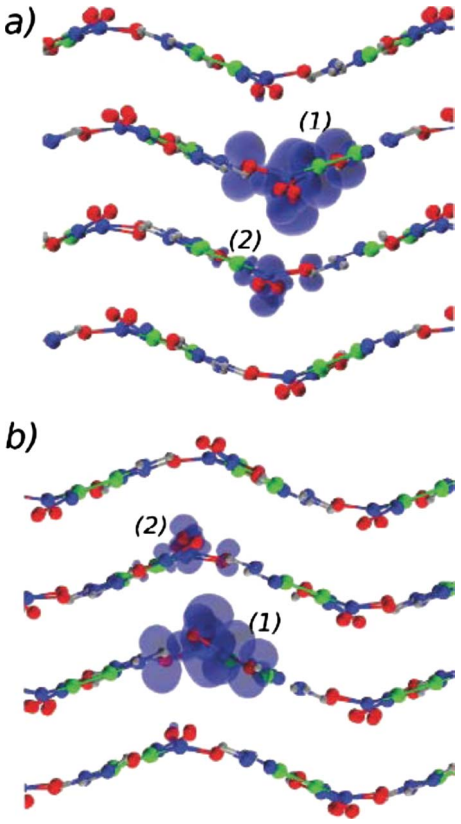

FIG. 7. (Color online) Spin-density plot of localized electron and hole polarons in DADNE crystal. (a) An extra electron localizes over two molecules (1) and (2) in neighboring layers. An electron occupies molecular orbitals of nitro groups; (b) a hole, similarly to an electron, localizes over two molecules in neighboring layers to minimize dipole moment of the system.

ized on the nitro groups of each of the two molecules 1 and 2 [see Fig. 7(a)].

The polaron-induced lattice deformation along the z axis (perpendicular to the layers) is relatively small, however, the two electron-bearing molecules move apart. This induces an increase in the distance between the carbons atoms bonded with the nitro groups by about 0.5 Å. The intralayer relaxation exhibits smaller shifts of molecules (0.25 Å) around the two molecules. The intralayer hydrogen bonds between uncharged and electron-bearing molecules are shortened from the distances characteristic for the neutral crystal 2.04/2.01–1.79/1.82 Å. This is due to the attraction between the protons and the oxygen atoms bearing the extra negative charge. Due to the asymmetric character of the extra electron localization, the local geometries of the molecules 1 and 2 also differ. The O-N bond in the molecule 1 is elongated from 1.31 to 1.33/1.36 Å. For the molecule 2 with only about 30% of the extra electron, there is almost no change in N-O bond length. At the same time the N-C bonds in both molecules become shortened from 1.4 to 1.35/1.39 Å, whereas the C=C bond length is decreased by 0.2 Å. The rotation angles of nitro groups with respect to the molecular plane increase by 12°/25° and 10°/13°. At the same time, ∠O-N-O and ∠N-C-N angles in both molecules are changed only within 2° with respect to the perfect geometry.

Ionization of perfect DADNE crystal leads to hole localization on the two neighboring molecules in adjacent layers. The spin density is again unequally distributed between the two molecules, with a larger density on the molecule 1 [see Fig. 7(b)]. The hole polaron occupies the nitro carbon and the nitro groups of the molecule 1 and polarizes one nitro group of the molecule 2 [see Fig. 7(b)]. This is accompanied by a split of a one-electron level, which is located inside the valence band in the perfect crystal, up from the top of the valence band by about 0.4 eV after the hole localization. The interlayer relaxation of the geometry along the z direction is negligible, except that the polaron-bearing molecules 1 and 2 shift toward each other: the distance between the carbon atoms in these molecules decreases from 4.41 to 4.12 Å, and the interlayer distance between the nitrogen atoms decreases by 0.42 Å. The intralayer relaxation is similar to that for the electron polaron: there are small interlayer displacements of molecules with respect to each other, which are facilitated by the flexibility of hydrogen bonds. Due to the lack of charge, the intermolecular attraction between the O atoms of molecules 1 and 2 and a respective proton of the nearest neutral molecule is weakened, which leads to a slight increase in the H-O distance to 2.06 Å. The intramolecular parameters are also affected by the presence of the trapped hole. The O-N bond lengths in the molecules 1 and 2 decrease by 0.1–0.2 Å, whereas the C-N bonds elongate by 0.3–0.4 Å, and the C=C distance increases by 0.2 Å. The intramolecular ∠O-N-O and ∠N-C-N angles change by only of 2°–3°.

B. ECM polaron calculations

In the ECM calculations we used a QM cluster including eight molecules [see Fig. 3(c)] surrounded by region I with the radius of 20 Å. The basis set for the ECM calculations is described above. These calculations gave very similar results—the extra electron is delocalized in the perfect lattice and becomes localized on the nitro groups of two molecules after the relaxation with self-trapping energy of about 0.5 eV. In ECM, the radius of the region where molecules are allowed to relax is much bigger than in the periodic calculations as it involves the whole region I. As has been shown,[54] defect-induced relaxation in solids formed by flexible networks can propagate far from a defect site. Analysis of the lattice distortion caused by the electron trapping shows that atomic displacements as large as 0.05 Å are still induced at the distance of about 15 Å from the defect center, i.e., much beyond the border of the QM cluster (11.5 Å). Not surprisingly, the lattice relaxation is mainly characterized by deformation and rotation of flexible nitro and amino groups. In the case of the electron polaron, the largest atomic displacements of the order of 0.17 Å correspond to nitro groups. They are caused by the fact that the extra electron localized on nitro groups strongly repels the surrounding nitro groups because their oxygen atoms bear a negative charge. At the same time, the amino groups are less affected by polaron localization: their largest displacements do not exceed 0.11 Å. Carbon atoms are perturbed the least and displaced only by ~0.04 Å.

The character of the intralayer relaxation is similar to that obtained via the periodic model. Indeed, hydrogen bonds be-

tween uncharged and electron-bearing molecules are shortening to 1.77/1.79 Å. Due to the presence of the localized negative charge, the local geometry of polaron-bearing molecules characterizes by shortening of C-N bonds on 0.1 Å and the elongation of O-N bonds on 0.4 Å. However, the rotation angles of nitro groups with respect to the molecular plane increase by 5°/20° and 6°/10°, i.e., less pronounced then in the periodic model.

ECM modeling of a hole polaron has also shown its delocalization in the perfect lattice. Relaxation of the lattice leads to localization of the polaron on two molecules in adjacent layers. However, the self-trapping energy of a hole, 1.2 eV, is larger than that found for electron polaron. The hole trapping induces a long-range relaxation of the lattice up to 11 Å with displacements of the molecules with respect to their initial positions. The distortion of polaron-bearing molecules is expressed by a rotation of nitro groups and slight elongation of carbon-carbon bonds. These results demonstrate that the boundary conditions in ECM do not affect the character of electron or hole localization. They do not, however, provide a proof of electron localization as the extent and character of electron localization is known to depend on the amount of Hartree-Fock exchange included in the hybrid B3LYP functional. We note that for smaller gap insulators, such as HfO_2[16], B3LYP tends to give more reliable predictions of the character of electron or hole localization than for wider gap oxides, such as MgO or SiO_2[16].

To test whether the charge localization obtained in DADNE is an artifact of the B3LYP functional, we carried out similar calculations for tetracene. This crystal has a very similar band gap (about 3 eV) and tetracene molecules also have double C=C bonds, however no lattice polaron (i.e., electron or hole localization) has been observed in this material.[10] Therefore, if using B3LYP would lead to artificial polaron localization, this would indicate that our predictions for DADNE could be also flawed. We used a $1\times2\times1$ B3LYP optimized supercell, with the parameters $a=8.60$ Å, $b=13.11$ Å, and $c=12.26$ Å. A distortion (elongation) in one of the C=C bonds was introduced as a precursor for the polaron state. The two C atoms have different environments, one of them being bonded to C and H atoms and the other being attached only to C atoms. An electron was added to the supercell to produce the polaron state and the excess charge was compensated by a charged background. Then, the system was allowed to relax to the minimum total energy. The resulting structure shows the electron delocalized among all the C atoms in the structure and no lattice polaron was formed, in agreement with experimental data.[55] This result suggests that the electron and hole localization obtained in DADNE using the B3LYP functional could be indeed a real effect.

V. SUMMARY AND CONCLUSIONS

We applied ECM to studying the proton transfer and electron and hole localization in DADNE. The problem of the hydrogen (or proton) transfer is as important as it is complicated and is far from solution and completion, equally in energetic solids and in other materials.[56,57] Our paper sheds some light on the mechanisms of the proton transfer and HONO-isomer formation in the chemical decomposition of DADNE. In particular, we demonstrate that HONO formation cannot be considered as a precursor for the thermal decomposition of crystalline DADNE. This suggests that the observed NO products in the course of thermal decomposition of solid DADNE (Refs. 44 and 45) should arise primarily from the nitro-to-nitrite isomerization[2,3,58] and H_2O most likely stems from secondary reactions. The obtained conclusions confirm that intermolecular interactions in the lattice are very important for describing these processes in a solid state.[56,58]

Our periodic and ECM calculations suggest that both electrons and holes can self-trap in DADNE. We predict that in static approximation using B3LYP functional, an extra electron or a hole can break the lattice translational symmetry, becoming localized at its self-induced local distortion. We did not study the polaron hopping between equivalent neighboring lattice sites, however, the relatively large self-trapping energies of about 0.5 eV suggest that it is a likely mechanism of conductivity at room temperature.

The results of this work demonstrate that the ECM method can serve as a useful tool for modeling chemical reactions, defect structures, and defect-induced processes in molecular crystals. It allows us to take into account both the short-range interaction between molecules and the long-range effects of the electrostatic potential and the defect-induced lattice distortion using a combination of quantum-chemical methods and classical force fields. Application of this method to a broad class of molecular materials can help to uncover details of the initiation of chemistry under a variety of conditions, including the presence of lattice imperfections, elevated pressure and temperature, and high radiation fields.

ACKNOWLEDGMENTS

This work is supported in part by the USA ARO MURI Grant No. W9011NF-05-1-0266 and ONR Grant No. N00014-09-1-0225. D.M.R. and P.V.S. were supported by the Grant-in-Aid for Creative Scientific Research under Grant No. 16GS0205 from the Japanese Ministry of Education, Culture, Sports, Science and Technology. The calculations were carried out using NERSC and UCL CRAG facilities. Authors are grateful to Betsy Rice for providing the initial FF potentials set. M.M.K. thanks the Office of the Director of National Science Foundation for support under the IRD Program.

*Present address: Department of Chemistry, University College London, Gower Street, London WC1E 6BT, United Kingdom.
†Present address: Department of Earth Sciences, University College London, Gower Street, London WC1E 6BT, United Kingdom.

[1] B. M. Rice and C. F. Chabalowski, J. Phys. Chem. A **101**, 8720 (1997); B. M. Rice and J. J. Hare, *ibid.* **106**, 1770 (2002); B. M. Rice, J. J. Hare, and E. F. C. Byrd, *ibid.* **111**, 10874 (2007).
[2] A. V. Kimmel, P. V. Sushko, A. L. Shluger, and M. M. Kuklja, J. Chem. Phys. **126**, 234711 (2007).
[3] A. Gindulyté, L. Masaa, L. Huang, and J. Karle, J. Phys. Chem. A **103**, 11040 (1999).
[4] P. Politzer, M. C. Concha, M. E. Grice, P. Lane, and D. Habibollazadeh, J. Mol. Struct.: THEOCHEM **452**, 72 (1998).
[5] C. Wu and L. E. Fried, J. Phys. Chem. A **104**, 6447 (2000).
[6] M. M. Kuklja and A. B. Kunz, J. Appl. Phys. **87**, 2215 (2000); M. M. Kuklja, Appl. Phys. A: Mater. Sci. Process. **76**, 359 (2003); M. M. Kuklja and S. N. Rashkeev, Phys. Rev. B **75**, 104111 (2007).
[7] K. Hannewald, V. M. Stojanovic´, J. M. T. Schellekens, P. A. Bobbert, G. Kresse, and J. Hafner, Phys. Rev. B **69**, 075211 (2004).
[8] S. Serra, S. Iarlori, E. Tosatti, S. Scandolo, M. C. Righi, and G. E. Santoro, Chem. Phys. Lett. **360**, 487 (2002). D. Ceresoli, E. Tosatti, S. Scandolo, G. Santoro, and S. Serra, J. Chem. Phys. **121**, 6478 (2004).
[9] A. K. Galwey, *Chemistry of Solids* (Chapman and Hall, London, 1967).
[10] E. A. Silinsh, in *Organic Molecular Crystals: Their Electronic States*, Springer Series in Solid-state Sciences, M. Cardona, P. Fulde, H.-J. Queisser, (Springer, Berlin, 1980).
[11] L. Caramella, G. Onida, F. Finocchi, L. Reining, and F. Sottile, Phys. Rev. B **75**, 205405 (2007).
[12] F. Bruneval, F. Sottile, V. Olevano, R. Del Sole, and L. Reining, Phys. Rev. Lett. **94**, 186402 (2005).
[13] O. Pulci, M. Marsili, E. Luppi, C. Hogan, V. Garbuio, F. Sottile, R. Magri, and R. Del Sole, Phys. Status Solidi B **242**, 2737 (2005).
[14] *Quantum Mechanical Cluster Calculations in Solid State Studies*, edited by R. W. Grimes, C. R. A. Catlow, and A. L. Shluger (World Scientific, Singapore, 1991).
[15] Y. Zhang, H. Lin, and D. G. Truhlar, J. Chem. Theory Comput. **3**, 1378 (2007).
[16] A. V. Kimmel, P. V. Sushko, and A. L. Shluger, J. Non-Cryst. Solids **353**, 599 (2007); D. Muñoz Ramo, A. L. Shluger, J. L. Gavartin, and G. Bersuker, Phys. Rev. Lett. **99**, 155504 (2007); K. M. Beck, M. Henyk, C. Wang, P. E. Trevisanutto, P. V. Sushko, W. P. Hess, and A. L. Shluger, Phys. Rev. B **74**, 045404 (2006).
[17] P. Maurer, A. Laio, and U. Rothlisberger, J. Chem. Theory Comput. **3**, 628 (2007).
[18] H. M. Senn and W. Thiel, Top. Curr. Chem. **268**, 173 (2007).
[19] B. Swerts, J. Van Droogenbroeck, A. Peeters, and C. Van Alsenoy, J. Phys. Chem. A **106**, 4245 (2002).
[20] P. Sushko, A. L. Shluger, and C. R. A. Catlow, Surf. Sci. **450**, 153 (2000); P. V. Sushko, A. L. Shluger, M. Hirano, and H. Hosono, J. Am. Chem. Soc. **129**, 942 (2007).
[21] N. V. Latypov, J. Bergman, A. Langlet, U. Wellmar, and U. Bemm, Tetrahedron **54**, 11525 (1998); U. Bemm and H. Östmark, Acta Crystallogr. C **54**, 1999 (1997); S. M. Peiris, C. P. Wong, and F. J. Zerilli, J. Chem. Phys. **120**, 8060 (2004).
[22] R. Dovesi, V. R. Saunders, C. Roetti, R. Orlando, C. M. Zicovich-Wilson, F. Pascale, B. Civalleri, K. Doll, N. M. Harrison, I. J. Bush, Ph. D'Arco, and M. Llunell, *CRYSTAL 2006 User's Manual* (University of Torino, Torino, 2006).
[23] A. S. Mysovsky, P. V. Sushko, S. Mukhopadhyay, A. H. Edwards, and A. L. Shluger, Phys. Rev. B **69**, 085202 (2004).
[24] R. Fletcher, Comput. J. **13**, 317 (1970); D. Goldfarb, Math. Comput. **24**, 23 (1970).
[25] J. Frisch *et al.*, *GAUSSIAN 03, Revision C.02* (Gaussian, Wallingford, CT, 2004).
[26] A. D. Becke, J. Chem. Phys. **98**, 5648 (1993).
[27] C. Lee, W. Yang, and R. G. Parr, Phys. Rev. B **37**, 785 (1988).
[28] M. A. Spackman and A. S. Mitchell, Phys. Chem. Chem. Phys. **3**, 1518 (2001).
[29] *Quantum Mechanical ab initio Calculations of the Properties of Crystalline Materials*, edited by C. Pisani (Springer, Heidelberg, 1996), p. 47; C. Roetti in *Quantum Mechanical ab initio Calculations of the Properties of Crystalline Materials*, edited by C. Pisani (Springer, Heidelberg, 1996), p. 125.
[30] A. B. Kunz, Phys. Rev. B **53**, 9733 (1996).
[31] M. M. Kuklja and A. B. Kunz, J. Appl. Phys. **89**, 4962 (2001).
[32] F. J. Zerilli and M. M. Kuklja, J. Phys. Chem. A **111**, 1721 (2007).
[33] M. Dion, H. Rydberg, E. Schröder, D. C. Langreth, and B. I. Lundquist, Phys. Rev. Lett. **92**, 246401 (2004).
[34] J. Hooper, V. R. Cooper, T. Thonhauser, N. A. Romero, F. Zerilli, and D. C. Langreth, ChemPhysChem **9**, 891 (2008).
[35] W. T. M. Mooij, F. B. van Duijeveldt, J. G. C. M. Van Duijeveldt-van de Rijdt, and B. P. van Eijck, J. Phys. Chem. A **103**, 9883 (1999).
[36] A. J. Du and A. C. Smith, Nanotechnology **16**, 2118 (2005).
[37] B. Rice, private discussion.
[38] A. E. Reed, R. B. Weinstok, and F. Weinhold, J. Chem. Phys. **83**, 735 (1985).
[39] D. C. Sorescu, J. A. Boatz, and D. L. Tompson, J. Phys. Chem. A **105**, 5010 (2001).
[40] M. M. Kuklja, F. J. Zerilli, and S. M. Peiris, J. Chem. Phys. **118**, 11073 (2003).
[41] J. D. Gale, J. Chem. Soc., Faraday Trans. **93**, 629 (1997).
[42] J. S. Murray and P. Politzer, J. Mol. Struct.: THEOCHEM **425**, 107 (1998); Theor. Chim. Acta **108**, 134 (2002).
[43] M. M. Kuklja, F. J. Zerilli, and P. Sushko, *Synthesis, Characterization, and Properties of Energetic/Reactive Nanomaterials*, MRS Symposia Proceedings Vol. 800, edited by R. W. Armstrong, N. N. Thadhani, W. H. Wilson, J. J. Gilman, Z. Munir, and R. L. Simpson, pp. 211–222 (2004).
[44] H. Östmark, A. Langlet, H. Bergman, N. Wingborg, U. Wellmar, and U. Bemm, in Proceedings of the 11th International Detonation Symposium, Snowmass, Colorado, 1998, ONR 33300-5 (Office of Naval Research, Arlington, VA, 2000), p 807.
[45] H.-X. Gao, F.-Q. Zhao, R.-Z. Hu, Q. Pan, B.-Z. Wang, X.-W. Yang, Y. Gao, and S.-L. Gao, Chin. J. Chem. **24**, 177 (2006).
[46] M. Iannuzzi and M. Parrinello, Phys. Rev. Lett. **93**, 025901 (2004).
[47] H. Jónsson, G. Mills, and K. W. Jacobsen, in *Classical and Quantum Dynamics in Condensed Phase Systems*, edited by B. J. Berne, G. Cicotti, and D. F. Coker (World Scientific, River Edge, NJ, 1998).
[48] T. Holstein, Ann. Phys. (N.Y.) **8**, 343 (1959).
[49] D. Emin, Adv. Phys. **24**, 305 (1975).

[50] M. M. Kuklja, E. V. Stefanovich, and A. B. Kunz, J. Chem. Phys. **112**, 3417 (2000).
[51] G. Pacchioni, F. Frigoli, D. Ricci, and J. A. Weil, Phys. Rev. B **63**, 054102 (2000).
[52] J. L. Gavartin, P. V. Sushko, and A. L. Shluger, Phys. Rev. B **67**, 035108 (2003).
[53] P. Durand and J. C. Barthelat, Theor. Chim. Acta **38**, 283 (1975).
[54] V. B. Sulimov, P. V. Sushko, A. H. Edwards, A. L. Shluger, and A. M. Stoneham, Phys. Rev. B **66**, 024108 (2002).
[55] J. Vilfan, Phys. Status Solidi **59**, 351 (1973).
[56] H. Chojnacki, Int. J. Mol. Sci. **4**, 408 (2003).
[57] A. V. Kimmel, P. V. Sushko, A. L. Shluger, and M. M. Kuklja, J. Phys. Chem. A **112**, 4496 (2008).
[58] M. M. Kuklja and S. Rashkeev, J. Phys. Chem. C **113**, 17 (2009).